Physics – Uspekhi **67** (11) 1139 – 1152 (2024)

REVIEWS OF TOPICAL PROBLEMS

PACS numbers: **07.57. – c**, **85.25. – j**, **95.55. – n**

55th ANNIVERSARY OF THE INSTITUTE OF SPECTROSCOPY
OF THE RUSSIAN ACADEMY OF SCIENCES (ISAN)

Superconducting terahertz receivers

L V Filippenko, A M Chekushkin, M Yu Fominsky, A B Ermakov,
N V Kinev, K I Rudakov, A V Khudchenko,
A M Baryshev, V P Koshelets, S A Nikitov

DOI: https://doi.org/10.3367/UFNe.2024.07.039726

Contents

Abstract. In some practical applications, devices based on superconducting electronics, due to their unique set of parameters, are far superior to those based on conventional technologies, being in some cases the only viable option. One of the most advanced areas is the development of ultra-sensitive terahertz-range receivers: their operating frequency has reached 1 THz, and the noise temperature is only limited by quantum or photon noise.

Keywords: radio astronomy, niobium-based high-quality tunnel junctions, low-noise SIS receivers, THz-range quantum-limited mixers

L V Filippenko [(1, a)], **A M Chekushkin** [(1, b)],
M Yu Fominsky [(1, c)], **A B Ermakov** [(1, d)],
N V Kinev [(1, e)], **K I Rudakov** [(1, 2, f)], **A V Khudchenko** [(1, 2, g)],
A M Baryshev [(3, h)], **V P Koshelets** [(1, 2, i)], **S A Nikitov** [(1, j)]
[(1)] Kotelnikov Institute of Radio Engineering and Electronics, Russian Academy of Sciences,
ul. Mokhovaya 11, korp. 7, 125009 Moscow, Russian Federation
[(2)] Astro Space Center, Lebedev Physical Institute, Russian Academy of Sciences,
ul. Profsoyuznaya 84/32, 117810 Moscow, Russian Federation
[(3)] Kapteyn Astronomical Institute, University of Groningen,
P.O. Box 72, 9700 AB Groningen, The Netherlands
E-mail: [(a)] lyudmila@hitech.cplire.ru, [(b)] chekushkin@hitech.cplire.ru,
[(c)] demiurge@hitech.cplire.ru, [(d)] ermakov@hitech.cplire.ru,
[(e)] nickolay@hitech.cplire.ru, [(f)] rudakov@asc.rssi.ru,
[(g)] khudchenko@asc.rssi.ru, [(h)] a.m.baryshev@gmail.com,
[(i)] valery@hitech.cplire.ru, [(j)] nikitov@cplire.ru

Received 9 March 2024, revised 17 May 2024
Uspekhi Fizicheskikh Nauk **194** (11) 1207 – 1222 (2024)
Translated by M Zh Shmatikov

1. Introduction

Due to the unique characteristics of superconducting elements, ultra-sensitive receiving systems can be created on their basis in an extremely wide frequency range [1–3]: magnetometers based on superconducting quantum interferometers (SQUIDs) [4–6] can measure ultra-low magnetic fields with frequencies starting from fractions of a hertz, and detectors based on superconducting tunnel junctions (STJs) make it possible to detect X-rays with an energy of several keV and gamma rays with an energy of tens of keV [7, 8]. The sensitivity of SQUIDs enables measuring fields at the level of 10^{-6} of the magnetic flux quantum Φ_0 and creating magnetoencephalographs for brain research [4, 5]; superconducting single-photon detectors (SSPDs) [9–11] can be used to detect single photons with a wavelength of less than 10 μm, and the energy resolution of the STJ is units of eV.

In addition, based on Josephson elements, a whole range of devices can be developed, intended not only for receiving signals but also for further processing of the received information. These include superconducting parametric amplifiers with a noise temperature significantly lower than the physical one [12–14] and information processing systems based on single-quantum digital devices (Rapid Single Flux Quantum, RSFQ) [15, 16]. It should be noted that the first RSFQ circuits were manufactured and studied at the Kotelnikov Institute of Radio Engineering and Electronics (IRE) of the Russian Academy of Sciences back in 1986 [17], and shortly after that an 8-bit superconducting analog-to-digital converter (ADC) was manufactured and tested [18]. Research into single-quantum digital devices was then successfully continued in many laboratories around the world. Currently being actively developed are interface

superconducting circuits of fast single-quantum logic for communication with quantum bits (qubits) and control of superconducting quantum systems at ultra-low temperatures [19, 20].

The development of ultra-sensitive receivers in the terahertz (THz) range is one of the most actively and successfully developing areas of superconducting electronics, where the potential of superconducting systems has been fully realized [21–25]. This is explained by both the extremely high nonlinearity of superconducting elements and their extremely low intrinsic noise due to the quantum nature of the elements and the cryogenic operating temperature, which makes it possible to create THz-range receiving systems with unique parameters unattainable for devices based on other principles. Since the accumulation time for receiving ultra-weak signals and detecting ultralow concentrations of substances is proportional to the noise temperature squared of the device used, receivers based on superconducting junctions make it possible to significantly reduce the observation time. Superconducting receivers are currently standard devices used in most ground- and space-based radio telescopes around the world, designed to explore fundamental issues related to the origin of the Universe. Many applications require a spectral resolution $\Delta f/f$ better than 10^{-6}; such a resolution can only be achieved using heterodyne receiving systems. A heterodyne mixer converts an incoming weak input signal to a lower intermediate frequency (IF) without phase loss; the spectrum of the IF signal is the same as the that of input signal, but shifted down in frequency by the local oscillator frequency.

Mixers based on superconductor–insulator–superconductor (SIS) tunnel junctions [21, 22, 26, 27] are the most sensitive input devices in heterodyne receivers at frequencies f ranging from 0.1 to 1.2 THz. The operation of the SIS mixer is based on the strong nonlinearity of the tunneling current on the current-voltage characteristic ($I-V$ characteristic) of the SIS junction; this nonlinearity is due to the tunneling of quasiparticles between two superconductors separated by a very thin oxide insulating layer. A quantum mechanical model [21, 26] is used to calculate the tunneling current under the action of the local oscillator signal; this process is called photon-induced stimulated tunneling. As a result of this process, quasiparticle-current steps appear on the $I-V$ characteristic of the SIS. By their nature, SIS mixers can provide gain conversion. Important advantages of SIS mixers are low power requirements for the local oscillator and very low intrinsic noise [21, 22, 26, 27]. The noise temperature of the mixer in the double-side band (DSB) mode is limited by the quantum value $hf/(2k_B)$ [28], where h and k_B are the Planck and Boltzmann constants, respectively. It is for this reason that SIS mixers have already been successfully used for both space missions and ground-based radio telescopes [23, 24, 29].

2. Tunnel SIS junctions

Tunnel SIS junctions are the main elements of most devices and circuits of superconducting electronics. To obtain tunnel structures, the applications of which are reviewed here, we used equipment that is part of the Unique Scientific Installation (USI) Cryointegral, a technological and measuring complex for the manufacture of superconducting nanosystems based on new materials [30], which was created at the Kotelnikov Institute of Radio Engineering and Electronics, Russian Academy of Sciences. This complex is a unique facility and, according to published data, the only one in Russia where high-quality niobium-based tunnel junctions can be produced. Over the past few years, a technology has been developed for the fabrication of $Nb-AlO_x-Nb$ tunnel junctions with high current density and low leakage [31–33]. On their basis, a technology was developed for producing multilayer chips containing up to 1000 elements; the technology was optimized to increase the degree of integration and yield of working circuits.

Several new technological processes and methods for producing superconducting tunnel junctions with record parameters have been developed. The established technology for manufacturing high-quality tunnel junctions has been used in a number of fundamental physical studies and experiments. In particular, this technology has been used to manufacture annular tunnel junctions withstanding more than 10,000 thermal cycles, which have been used to explore spontaneous symmetry breaking by forming fluxons during a rapid transition through the critical temperature of a tunnel structure (Zurek–Kibble mechanism) [34]. Using this technology, ultra-sensitive SQUID magnetometers [6, 35] and elements of metamaterials based on superconducting quantum interferometers have been developed and successfully implemented; metamaterials with tunable negative magnetic permeability have been created and their characteristics measured [36, 37].

2.1 $Nb-AlO_x-Nb$ tunnel junctions

To achieve the performance limits of receiving systems, SIS tunnel junctions with an extremely low leakage current below the gap voltage V_g and minimal spreading of the energy gap δV_g are required. This is especially important for low-frequency devices ($f < 300$ GHz), since δV_g should be much smaller than the size of the quasiparticle step hf/e, and the leakage current at a bias voltage of about $V_g - hf/2e$ (in the middle of such a step) determines the mixer noise. A well-proven technology for the production of $Nb-AlO_x-Nb$ tunnel junctions is based on the capability of a very thin Al layer (5–7 nm thick) to completely cover the base Nb electrode, effectively planarizing the columnar microstructure of the Nb film. This Al layer is subsequently oxidized, and then the upper Nb electrode is deposited on the oxidized layer, forming the so-called three-layer structure [38, 39].

Due to the proximity effect and the presence of a normal aluminum layer near the tunnel barrier, a well-pronounced knee-shaped structure appears on the $I-V$ characteristics of the $Nb-AlO_x-Nb$ junctions at voltages slightly above V_g (Fig. 1a). The exact shape of the $I-V$ characteristic of the $Nb/Al-AlO_x/Nb$ ($S-S'/I/S$) tunnel junction depends on the density of states of the quasiparticles in the S' layer (Al). This density of states for Nb/Al bilayers was calculated using the microscopic proximity effect model [40]. The model assumes a small mean free path of electrons (dirty limiting conditions) in both S (Nb) and S' (Al) materials. The dependence of this effect on the parameters of the tunnel structure was experimentally studied in [41]. The presence of a knee-shaped structure on the $I-V$ characteristic leads to features on the quasiparticle steps (Fig. 1a), which in turn leads to instability and nonlinearity of the mixer operation at some frequencies.

To obtain a knee-free $I-V$ characteristic, the Al layer thickness must be minimal ($d_{Al} < 3$ nm). An aluminum layer this thin cannot continuously cover the surface of the lower

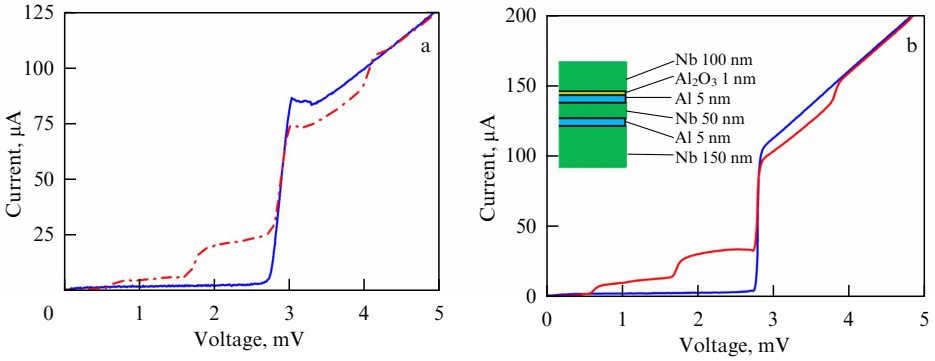

Figure 1. Experimental current–voltage characteristics of mixing elements: (a) Nb–AlO_x–Nb SIS junction manufactured using conventional technology; (b) Nb/Al/Nb–AlO_x–Nb SIS junction with an additional Al interlayer. Solid curve shows autonomous current–voltage characteristics. Dashed-dotted line shows current–voltage characteristics under the effect of a local oscillator at a frequency of 262 GHz at optimal power.

electrode, which is formed by a thick 200-nm Nb film, having a columnar structure [42, 43]. A thin Nb electrode ($d_{Nb} < 50$ nm) has a smoother surface and is completely wetted by Al down to a thickness of $d_{Al} = 3$ nm, the R_j/R_n ratio (the quality parameter defined as the ratio of the below-gap resistance to the normal resistance) remaining at about 40 for all aluminum thicknesses used [41]. SIS junctions with a thin lower electrode feature an almost ideal $I-V$ characteristic, but are of little use for high-frequency applications, since $d_{Nb} < \lambda_{Nb} = 90$ nm (the penetration depth of the magnetic field), which significantly increases the inductance of microwave elements. To resolve this problem and realize knee-free junctions with a thick lower electrode, structures with an additional Al interlayer in the lower Nb electrode were proposed [41]. Then, the order parameter in the thin Nb–Al bilayer becomes spatially uniform and the density of states is close to that predicted by the Bardeen–Cooper–Schrieffer theory (BCS). Thus, in the Nb/Al_{add}/Nb_{add}–Al/AlO_x–Nb structure, the knee disappears, and the $I-V$ characteristic becomes close to ideal. The obtained results demonstrate the possibility of 'tuning' the shape of $I-V$ characteristics of tunnel junctions by selecting the thickness of the layers in the composite lower electrode. The current–voltage characteristic of the Nb/Al/Nb–AlO_x–Nb mixing element (with an area of about 1 μm^2) with an additional Al layer in the lower electrode, measured in the voltage bias mode, is shown in Fig. 1b; the critical current of the SIS junction is suppressed by a magnetic field [33]. The normal resistance of the SIS junction $R_n = 22$ Ω; the quality factor, characterized by the ratio of the below-gap resistance to the normal R_j/R_n, reaches 40; the value of the energy gap $V_g = 2.8$ mV; and the spreading of the gap feature δV_g is approximately 0.1 mV. These are the characteristics required to create receiving systems with a quantum limited noise level.

2.2 Nb–AlN–NbN tunnel junctions

Junctions with a high tunnel current density allow increasing the operating frequency of SIS receivers and expanding their bandwidth. However, there is a limit to enhancing the barrier transparency for SIS junctions based on aluminum oxide. This limit is about 10–15 kA cm^{-2}; with a further increase in current density, the quality of the junctions sharply deteriorates. To overcome this limitation, a technology was developed for manufacturing Nb–Al/AlN–Nb tunnel SIS junctions with extremely high transparency of the tunnel barrier by nitriding the Al surface in a plasma RF discharge. Such SIS junctions feature a fairly good ratio $R_j/R_n > 10$ at very high current densities of up to 100 kA cm^{-2} [44, 45].

The parameters of tunnel structures were further improved by developing a technology for manufacturing circuits based on three-layer Nb–AlN–NbN structures, where niobium nitride instead of niobium is used as the top electrode [46, 47]. The use of such structures makes it possible not only to enhance the tunnel current density but also to significantly increase the total gap voltage V_g of the junction from 2.8 to 3.7 mV. This advancement significantly increases the operating potential of structures at high frequencies (over 700 GHz), when the size of the hf/e photonic step exceeds V_g. In addition, at high current densities for Nb–AlN–NbN junctions, the quality parameter determined by the ratio of the below-gap resistance to the normal resistance, R_j/R_n, turns out to be noticeably larger than for purely niobium junctions [33, 46, 47] (Fig. 2). The R_j/R_n ratio reaches 20 at a tunnel current density of 70 kA cm^{-2}, which indicates the high quality of the tunnel barrier obtained by nitriding a thin aluminum film in a high-frequency plasma discharge (Fig. 3a) [46, 47]. All these advancements made it possible to increase the operating frequency of SIS receivers, expand their band, and create ultra-sensitive receivers operating in the 100–1000 GHz range. However, to ensure good matching between junctions with such a high current density and the antenna, submicron SIS junctions are needed.

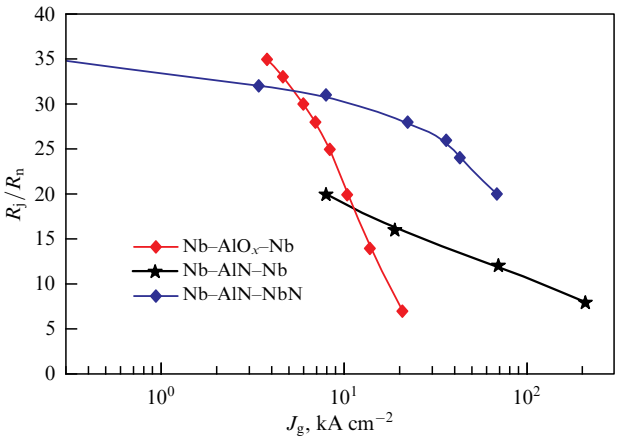

Figure 2. Quality parameter R_j/R_n as a function of density of tunneling current in SIS junctions of various types [47].

2.3 Electron beam lithography

Electron beam lithography (EBL) is one of the most promising methods for producing nanostructures intended for research purposes, since it allows rapid changes in the design of individual elements and the microcircuit as a whole and provides high reproducibility of results in the submicron region of tunnel junction sizes [48]. Submicron SIS junctions can be produced by direct lithography — direct exposure of the sample surface using EBL. The advantages of electron lithography are high resolution and the ability to quickly alter exposed structures by simply modifying the computer program. The alignment of the topology pattern on adjacent fields within one process layer is ensured by a precision measuring system based on a laser interferometer. The design of the microstructure topology should be developed in such a way that the circuit elements with critical dimensions do not fall on the field boundaries. For electron exposure, a Raith e_LiNE lithograph with a maximum processing field of the electron-optical system of 1000×1000 μm was used [49, 50].

Electron resists are used as a mask for forming structures for metal deposition [48]. For positive resists, exposure to an electron beam decreases its molecular weight when the bonds between molecules are broken, increasing their solubility. For negative resists, irradiation stimulates the formation of cross-links in polymer molecules. As a result of the electron beam scattering in the resist, a distribution of molecular masses is established which increases from the beam axis to the edge. It generates a corresponding contrast γ, which is the response of the resist to the electron beam and is determined by the distortions introduced by the resist and the substrate. The developer actually reveals the distribution of the beam intensity and the distortions introduced by the unevenness of the beam intensity and the radiation scattered (directly and inversely) in the resist.

To develop a reproducible and reliable technology for manufacturing high-quality tunnel structures with good reproducibility and a small spread of parameters over the substrate, a technology for manufacturing submicron-sized Nb–AlN–NbN tunnel structures using direct EBL methods and subsequent plasma-chemical etching was developed and approved. The SIS junction is formed by etching a three-layer Nb–AlN–NbN structure through a mask in a resist film formed using electron lithography [51].

2.4 NbTiN/Nb–AlN–NbN/Al structures

The operating frequency of SIS receivers based on niobium films is limited by the Nb energy gap frequency (approximately 700 GHz). A solution to this problem was found in the creation and use of devices with microstrip lines based on Nb compounds with higher energy gap frequencies; in particular, NbTiN is used to this end. The upper electrode of the microstrip line is usually made of a metal that is normal at these temperatures (usually Al) to avoid overheating of the SIS junction [52–54]. We developed an SIS mixer based on Nb–AlN–NbN tunnel junctions with a high critical current density, built into a microstrip line consisting of a 320-nm-thick NbTiN lower electrode (ground plane) and a 500-nm-thick Al upper electrode [55]. The microstrip electrodes are separated by a 250-nm-thick SiO_2 insulating layer. The SIS junction is located on the NbTiN film, while the upper NbN layer contacts the upper Al electrode (see the cross section of the structure in Fig. 3b).

3. SIS receivers for radio astronomy

The development of ultra-sensitive THz receivers is arguably the best known (and most successful) direction in the development of superconducting electronics. Receiving systems for the largest modern radio astronomy project, the multi-element interferometer Atacama Large Millimeter/submillimeter Array (ALMA) [23] and the Herschel Space Observatory program [24], were created based on superconducting structures. The importance of this research area was recently confirmed by the publication of the first ever 'image' of a supermassive black hole in the center of the M87 galaxy [56, 57]. This event widely resonated in the scientific community, comparable to the discovery of gravitational waves. Black holes are extremely compact, so their observation requires ultrahigh angular resolution. Research is currently being conducted as part of the ground-based Event Horizon Telescope (EHT) projects [58]; new sites for very-long-baseline interferometry are being created, including in Argentina (Large Latin American Millimeter Array, LLAMA) [59] and Namibia (Africa Millimetre Telescope, AMT) [60]; active research is being conducted to create a submillimeter observatory in Russia. The highest angular resolution will be attained in the Russian space agency's Millimetron project to create a space–Earth radio interferometer with a base of 1.5 mln km [61, 62].

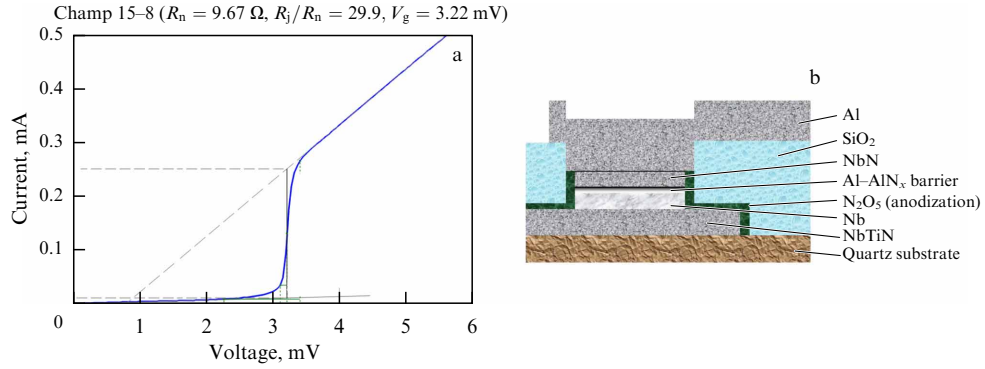

Figure 3. (a) Current–voltage characteristic of a twin Nb–AlN–NbN mixer produced on a quartz substrate (area of each SIS junction $S = 0.37$ μm^2, $V_g = 3.22$ mB, $R_nS = 7$ Ω μm^2, tunneling current density $J_g = 34$ kA cm^{-2}). Critical current is suppressed by the magnetic field. (b) Sectional view of receiving structure based on Nb–AlN–NbN tunnel junction with a high critical current density, built into a microstrip line consisting of a lower NbTiN electrode and an upper Al electrode.

The Millimetron space observatory also features unique scientific potential for studying the Universe in the single-telescope mode, since measurements will not be limited by atmospheric absorption in the terahertz frequency range. To equip these telescopes with world-class scientific instruments, superconducting structures with a unique set of parameters are required that meet the needs of space and ground missions. The use of state-of-the-art nanoelectronics methods allows the implementation of superconducting integrated structures and receivers based on them for operation in the terahertz spectral region with limiting (quantum) sensitivity. This section describes the receiving systems for two frequency ranges for the Millimetron space observatory; in particular, the SIS receiving elements of the 210–275-GHz range with a double-sideband noise temperature of less than 20 K, which is only 1.5 times higher than the quantum limit hf/k_B and lower than the best results known to date. We also present the results of studying receivers with an operating frequency of up to 950 GHz.

3.1 SIS mixer for 210–275-GHz range

A modular design was applied in the design of the mixer unit for the 210–275-GHz frequency range; this approach was developed and tested when creating the Band 9 receivers for the ALMA radio interferometer [63]. The mixer unit (Fig. 4) [33] consists of several separate elements: an input horn (*1*), a central unit with a waveguide (*2*), a replaceable rear block with a waveguide shorting (*3*), in which the mixer chip is installed, and a block with two magnetic pins for suppressing the Josephson current of the SIS junction (*4*). The receiving chip (150 μm wide) is located in a rectangular waveguide measuring 1000 × 500 μm at a distance of 230 μm from the rear part of the waveguide, orthogonal to the direction of propagation (Fig. 5a, b) [33]. The $Nb-AlO_x-Nb$ SIS junction is placed in a planar $Nb/SiO_2/Nb$ tuning structure produced on a 125-μm-thick quartz substrate. Low-pass blocking filters were used to prevent leakage of the high-frequency input signal through the dielectric-filled waveguide formed by the quartz substrate in the metal channel (Fig. 5b).

To achieve the performance limit of the mixer, the tunnel SIS junction must be efficiently matched to the input waveguide impedance at high frequencies and to the 50-Ω amplifier impedance over the entire intermediate frequency band. A waveguide probe and tuning structure were used to match the waveguide impedance of approximately 400 Ω to the high-frequency impedance of the SIS. A combination of a CoPlanar Wavequide (CPW) and a MicroStrip Line (MSL) was used to tune the intrinsic capacitance of the SIS tunnel

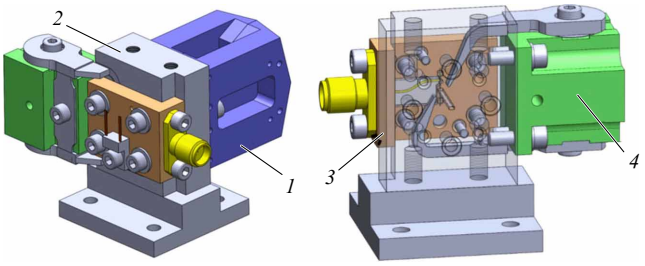

Figure 4. 3D model of a mixer unit for frequency range of 210–275 GHz: *1* — input horn, *2* — central unit with a waveguide, *3* — rear part with a mixer chip, *4* — magnetic block for suppressing Josephson effect [33].

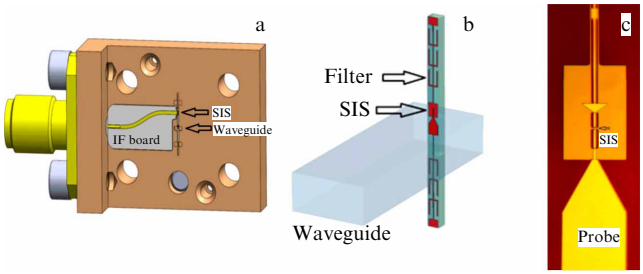

Figure 5. Details of a mixer for the range of 210–275 GHz: (a) 3D model of contactor unit with a board for IF matching. Arrows in figure indicate mixing SIS junction and waveguide; (b) 3D model of mixing SIS element based on a double-sided chip placed inside waveguide channel. Input horn is located on front side of waveguide mixer unit; (c) image of central part of mixing SIS element [33].

junction and match the resulting impedance of the SIS structure to the waveguide at high frequencies (Fig. 5c). This approach allowed the tuning structures to be made more compact. Since the wavelengths in the tuning lines in the IF range significantly exceed the structure dimensions, the microstrip tuning lines add some capacitance to the sample impedance at the IF. To match the output impedance of the mixer to the amplifier, a matching structure can be used. In [33], we used a printed circuit board with a 50-Ω line without any additional tuning elements (Fig. 4a).

The Michelson Fourier transform spectrometer (FTS) method was used to estimate the frequency range of the SIS mixer matching. A broadband source of sub-terahertz radiation (a black body heated to 1500 K) was matched with the FTS, in which an SIS mixer was used as a detector. The voltage on the mixer was chosen slightly below the gap voltage; the DC response was measured as a function of the position of the movable mirror. The Fourier transform can be applied to these data to obtain the characteristic of matching the mixer with radiation in the required frequency range. The experimental data demonstrate good matching of the mixer in the range from 210 to 280 GHz, in full agreement with the results of numerical simulation.

When local oscillator power of frequency f is applied, quasiparticle steps appear on the $I-V$ characteristic of the SIS mixer, which are due to tunneling of quasiparticles under the action of radiation (Fig. 6a); the size of these steps, which is measured from the gap voltage, is equal to hf/e. The operating point of the mixer is chosen in the middle of such a step; the Josephson effect leads to the appearance of additional noise features on the $I-V$ characteristic; therefore, it is suppressed by a magnetic field. The mixer noise temperature in the dual-sideband mode was determined by the standard Y-factor method, at which the IF response is measured at two different load temperatures at the receiver input. The 'hot' load was an absorber at room temperature (295 K), while the 'cold' load was a liquid nitrogen-cooled absorber (78 K). The Y-factor was determined by subtracting the IF responses, in dB, for the hot and cold loads. Figure 6b shows the receiver Y-factor versus bias voltage, measured for a 241-GHz local oscillator with an IF of 6.5 GHz (IF filter bandwidth: 60 MHz). The best-case Y-factor is 5 dB, which corresponds to a receiver noise temperature of about 22 K. The noise temperature T_n (Fig. 7 [33, 64]) was obtained without any corrections for beam splitter and cryostat window losses; the T_n is only twice as high as hf/k_B in the

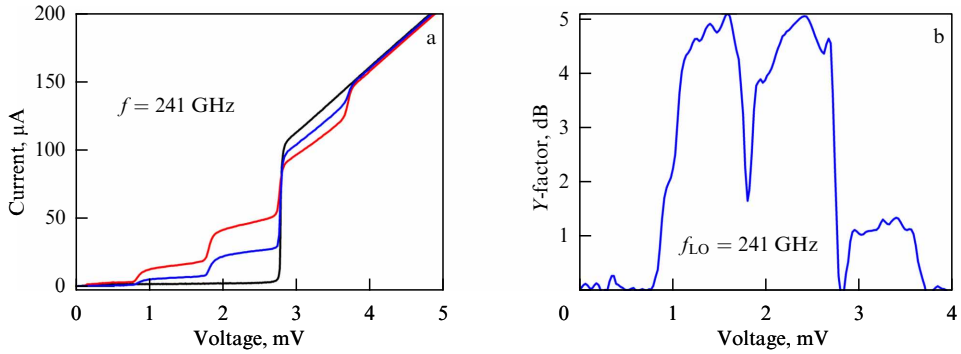

Figure 6. (a) $I-V$ characteristic of SIS mixer pumped at 241 GHz for two power values [33]. (b) Dependence of response (Y-factor) on voltage on SIS mixer [33].

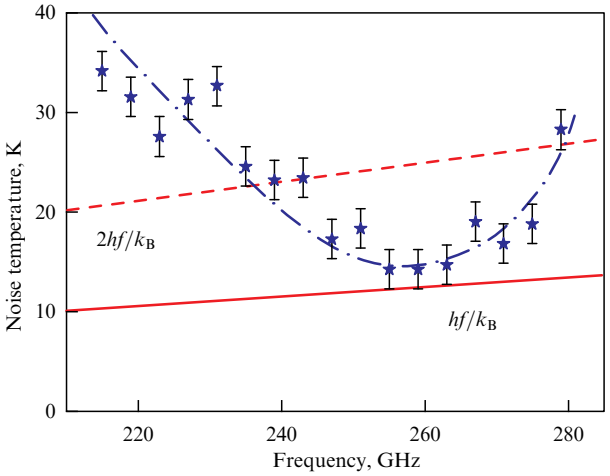

Figure 7. Noise temperature of mixer in double-sideband (DSB) mode [33].

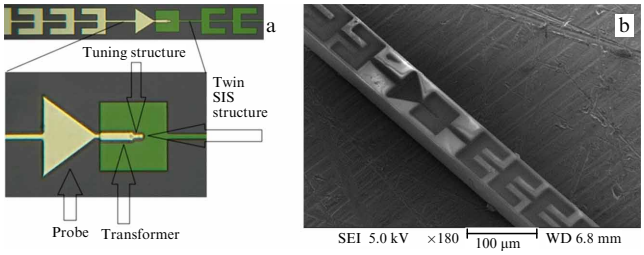

Figure 8. Schematic (a) and SEM image (b) of high-frequency SIS mixer for the CHAMP+ project. Central part of chip (including twin SIS junction, transformer, and probe) is enlarged [33].

frequency range from 240 to 275 GHz. The values obtained correspond to the technical requirements for the 210–275-GHz receiver of the Millimetron space radio telescope.

A detailed discussion of the contributions of individual components to the final noise temperature of the SIS mixer is presented in [64]; the estimates of the contributions can be summarized as follows [33]: (a) the 6-μm-thick Mylar beam splitter contributes 0.6 K to the mixer temperature; (b) the receiver input window, 0.5 K; and (c) the IF path (which is a combination of a Pamtech 4–12 GHz cryogenic isolator and a cryogenic amplifier), 6 K. Note that the quantum limit for the SIS mixer in double-sideband (DSB) mode is $hf/2k_B$ [28], which corresponds to 5.8 K at a frequency of 250 GHz. The stability of the receiver was assessed in [33] by recording the time dependence of the receiver output signal under the same operating conditions as for the noise temperature measurement; a 60-MHz bandpass filter was used to limit the signal bandwidth. The Allan dispersion time measured at a local oscillator frequency of 241 GHz reached 10 s [64], which is determined by the stability of all receiver components and is sufficient for radio astronomical measurements both on ground-based radio telescopes and aboard the space observatory.

3.2 SIS mixer for 700–950-GHz range

To create a broadband receiver for the 790–950 GHz range for CHAMP+, we used twin SIS junctions [65, 66] (each with an area of 0.5 μm^2 (Fig. 8)), coupled by a waveguide probe to the electric component of the field of a rectangular waveguide measuring 300 × 75 μm. For the SIS mixer [67, 68], high-current-density Nb–AlN–NbN tunnel junctions were used, included in a NbTiN–Al microstrip line [55]. The microstrip electrodes (the lower electrode made of NbTiN with a thickness of 320 nm and the upper electrode made of Al with a thickness of 500 nm) were separated by a 250-nm-thick SiO_2 insulator.

Since the tunnel junction resistance R_n decreases exponentially with decreasing barrier thickness, and the capacitance C increases linearly, SIS junctions with an AIN barrier, which allow achieving a high tunnel current density, make it possible to realize a higher $1/R_nC$ value, which provides a wider reception band. The 'twin' mixer circuit was realized using two SIS junctions located at a distance of 6.5 μm from each other and built into a 4.5-μm-wide microstrip line. The receiving structure was connected to the antenna using an impedance transformer measuring 7 × 27 μm [64], designed to match the junctions with a high current density with the waveguide probe (see Fig. 8).

Using SIS junctions with an AlN barrier allows obtaining high-quality tunnel structures (the ratio of the below-gap resistance to the normal one exceeds 20) for a high tunnel current density of up to 30 kA cm^{-2}. As a result, not only was a wide operating range of the receiver (from 675 to 950 GHz) realized, but so was a noise temperature that did not exceed $3hf/k_B$ at the best points (Fig. 9a). The figure shows the noise temperature in the dual-sideband (DSB) mode for three SIS mixers as a function of frequency. The noise temperature was corrected taking into account the losses in the input window and the beam splitter.

The developed receiving structures were used to upgrade the high-frequency receivers of the 7-pixel matrix for the CHAMP+ device installed on the APEX (Atacama Pathfinder Experiment) telescope; the input frequency range

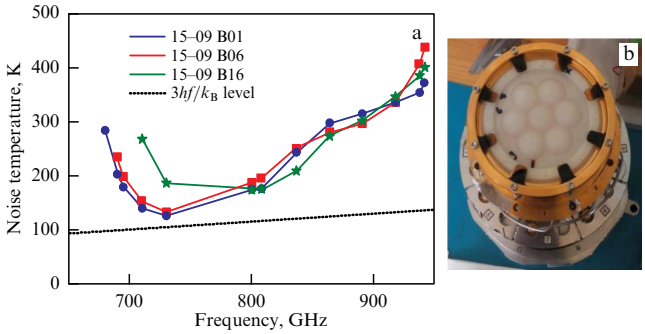

Figure 9. (a) Noise temperature in double-sideband (DSB) mode for three SIS mixers as a function of frequency. Dotted line shows noise temperature corresponding to $3hf/k_B$ [33]. (b) Image of 7-pixel SIS mixer array for high-frequency (790–950 GHz) CHAMP+ receiver on APEX radio telescope with a lens system in the upper part of cartridge body [33].

is 790–950 GHz, and the IF range is 4–12 GHz (Fig. 9b). The use of Nb–AlN–NbN structures included in the NbTiN/Al line [54, 64, 68, 69] made it possible to enhance the CHAMP+ sensitivity in the high-frequency range by a factor of 1.3 to 1.5 [69]. Under good weather conditions, with an atmospheric transparency of about 50% [70], the mapping rate of radio astronomical sources will be improved by about 40%. The developed SIS mixers can also be used for the Chinese observatory located in Dome A (Antarctica), for the Brazilian LLAMA telescope located in the Andes, and for the Millimetron space observatory (in the single telescope mode).

4. Integrated receiving structures

A whole range of elements and devices operating in the THz range and featuring a wide functionality can be created based on superconducting tunnel junctions. They include not only the highly sensitive receiving elements described in the previous section but also superconducting local oscillators (SLOs) in the THz range [47, 71–73] and harmonic mixers for measuring the SLO spectrum and synchronizing it with a reference synthesizer to implement the phase-locked loop (PLL) mode [73, 74], as well as cryogenic phase detectors [75, 76]. Moreover, the advanced technology for manufacturing superconducting integrated circuits [31, 32, 47] makes it possible to combine all of the listed elements on a single substrate and implement a fully superconducting integrated receiver (SIR) in the THz range [47, 72, 77]. This section contains a description of the main elements of the SIR and examples of its successful application both aboard a high-altitude balloon for studying the Earth's atmosphere [47, 72, 78, 79] and in the laboratory for measuring the radiation of new THz-range generators [80] and gas absorption spectra [81] and studying sub-THz radiation of the human body under physiological stress [82].

4.1 Superconducting heterodyne generator

Research into the options for using Josephson junctions to generate high-frequency electromagnetic radiation began soon after the discovery of the Josephson effect [83–85]. One of the most studied of them is the distributed Josephson junction (DJJ) with a length much greater than the penetration depth of the magnetic field into the junction. The DJJ is a long tunnel SIS junction in which the applied magnetic field and bias current create a unidirectional flow of Josephson vortices [2, 3, 47, 72, 86–89], each of which contains one quantum of magnetic flux $\Phi_0 = h/2e \approx 2 \times 10^{-15}$ Wb. Such generators based on the flow of Josephson vortices are called 'flux-flow oscillators' (FFOs). To create a constant magnetic field applied to the DJJ, an external solenoid or a built-in field control line is used, through which I_{CL} flows. When the Josephson vortex leaves the junction, a single-quantum voltage pulse is generated, the radiation frequency being related to the voltage across the junction V_{DC} by the fundamental Josephson relation $f = (2\pi/\Phi_0)V_{DC}$, with a coefficient which is about 483.6 GHz mV^{-1}. The velocity and flux density of the Josephson vortices and, consequently, the power and frequency of the emitted signal can be controlled independently by simultaneously setting the bias current and magnetic field.

To study the DJJ, integrated circuits were created containing a broadband detector based on the SIS junction matched with the DJJ [71–74]. A typical set of current–voltage characteristics of the DJJ, measured at various magnetic fields, is displayed in Fig. 10. Concurrently with the recording of the $I-V$ characteristics of the DJJ, the pumping of the SIS detector is measured, the level of which is shown in color. The pumping level criterion is the change in the tunneling current I_p at voltages slightly below the gap one (Fig. 11) due to the stimulated tunneling of quasiparticles. The value of I_p is usually normalized to the current step at the gap voltage I_g; the optimal value for the SIS mixer operation is $I_p/I_g = 0.25$. Figure 10 shows that a value of I_p/I_g greater than 0.25 is realized for DJJ voltages from 0.82 to 1.45 mV, which corresponds to the frequency range of 400–700 GHz. A set of $I-V$ characteristics of the SIS detector, measured at various values of the frequency and output power of the DJJ, is displayed in Fig. 11. It should be noted that the operating range of the SIS junction pumping is limited by the structure of the matching circuit (its topology and materials), rather than by the DJJ itself.

In the $I-V$ characteristic of the DJJ (see Fig. 10), several regions with different operating modes of the superconducting generator can be distinguished. At low magnetic fields, the distance between the vortices is large, and they interact weakly; with an increase in the applied magnetic field, the $I-V$ characteristic shifts linearly toward higher voltages. A powerful broadband 'noise' signal is generated [90]. As the magnetic field increases, a transition to the resonant flow

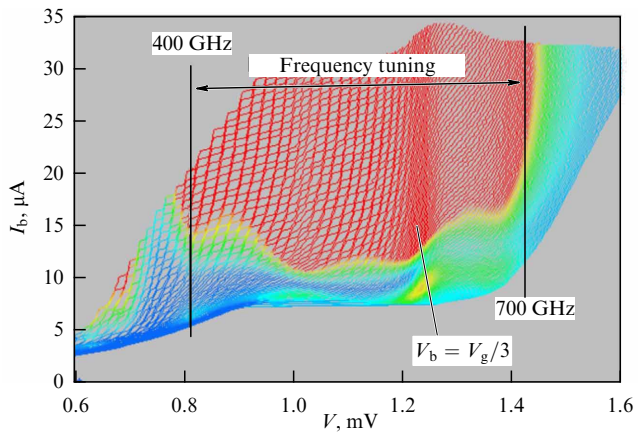

Figure 10. Set of DJJ $I-V$ characteristics measured at various magnetic fields. Color indicates pumping level of SIS detector at a given operating point [72].

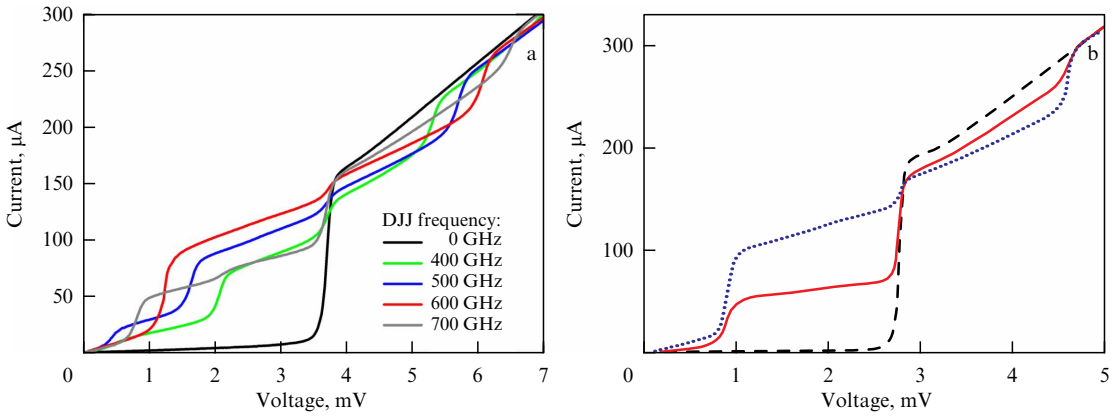

Figure 11. (a) Set of $I-V$ characteristics of SIS detector in the absence of a DJJ signal (black curve) and with pumping by a DJJ signal at various frequencies (colored curves) [46, 72]. (b) $I-V$ characteristics of SIS detector with pumping by a DJJ signal at a frequency of 470 GHz at two power levels [72].

mode of Josephson vortices occurs; a set of clearly defined Fiske steps appears on the $I-V$ characteristic, which is due to the influence of the reflected electromagnetic wave on the entering of vortices into the junction.

The resonant mode is realized up to the 'boundary' voltage V_b, at which the Fiske steps disappear. The boundary voltage V_b, which is equal to a third of the gap voltage, is about 0.95 mV for DJJs based on Nb–AlO_x–Nb SIS junctions and 1.2 mV for those based on Nb–AlN–NbN. Such a transformation of the DJJ operating mode is explained by the effect of self-action of Josephson radiation generated in the junction on the junction itself [91–93], which leads to stimulated tunneling of quasiparticles under the action of Josephson radiation from the DJJ. The effect manifests itself in a sharp increase in the quasiparticle current (and hence enhanced attenuation) at self-pumping voltage values $V_{SC} = V_g/(2n+1)$, which gives $V_g/3$ for $n = 1$; its value increases with the current density DJJ. This effect explains well not only the presence of current jumps on the $I-V$ characteristic at the 'boundary' voltage but also the rapid smoothing out of the Fiske steps (disappearance of the resonance mode) at voltages above $V_g/3$, which is due to an increase in the internal attenuation in the long junction [93]. Geometric resonances (Fiske steps) can only exist at low normalized attenuation, $\alpha l < 1$, where $l = L/\lambda_J$ is the junction length normalized to the Josephson length λ_J.

Starting from the very first experimental implementation of the DJJ, its theoretical description was limited to the phenomenological sine-Gordon equation. This model can qualitatively describe topological excitations in Josephson junctions, but fails to establish a quantitative relationship between tunneling currents and electromagnetic radiation. Developed in [94–96] was a microscopic model of DJJ operation, where it became possible to calculate the processes in the junction, taking into account the energy gap of superconductors. This approach, based on the theory of microscopic quantum tunneling, describes the essential features of real systems both in symmetric Nb–AlO_x–Nb structures and in asymmetric Nb–AlN–NbN junctions; this was confirmed by comparing the calculated current–voltage characteristics with experimental results [94, 95].

To measure SLO emission spectra, a superconducting integrated circuit was developed containing a DJJ, an SIS mixer, and elements for matching them at high frequencies (250–750 GHz). The DJJ output signal is fed to a harmonic mixer (HM), which is an SIS mixer with an area of about 1 μm^2, operating in the mode of mixing the DJJ signal with the nth harmonic of an external microwave source (synthesizer) with a frequency f_S of about 20 GHz. To prevent the synthesizer signal from reaching the DJJ, a high-pass filter with a lower pass limit of about 200 GHz is provided in the path between the DJJ and the HM. The output HM signal at the intermediate frequency $f_{IF} = \pm(f_{DJJ} - nf_S)$ is amplified by a cascade of amplifiers: first by a cryogenic microwave amplifier with a noise temperature of about 5 K and a gain of about 30 dB, then by an amplifier operating at room temperature with a gain of about 60 dB. Part of the IF signal is sent through a directional coupler to a spectrum analyzer, which is phase locked with the synthesizer; this allows the linewidth of the DJJ generation in the frequency range from 250 to 750 GHz to be measured with high accuracy [71–74]. The dependence of the SLO generation linewidth on its geometry and parameters was studied in detail, and the design and topology of the DJJ were optimized. Such developments made it possible to implement continuous frequency tuning of the superconducting generator in the entire operating range with an emission linewidth for optimized DJJ designs of less than 10 MHz (Fig. 12).

The developed integrated circuit can be used not only for measuring the SLO spectrum but also for stabilizing its frequency using a phase-locked loop [71–74]. In the PLL system, the IF signal is compared in a frequency-phase discriminator with a 400-MHz reference signal phase-locked to a 20-GHz synthesizer. An output signal proportional to the phase difference is fed back through a bandwidth regulator (with a maximum bandwidth of about 20 MHz) and fed to the DJJ through a 50-Ω 'cold' resistor mounted on the bias board of the integrated circuit. To accurately measure 'natural' DJJ linewidth, the IF spectra are averaged up to 100 times using frequency stabilization with a sufficiently narrow signal bandwidth (< 10 kHz). Narrowband feedback eliminates low-frequency drift and interference without affecting the linewidth and shape, which are determined by the nonlinear superposition of thermal and shot noise [71–74]. When the effective width of the fluctuation spectrum exceeds the self-consistent linewidth of the emission, the DJJ spectrum in the stand-alone mode has a Lorentzian shape (Fig. 12a, blue curve). A PLL can significantly narrow the DJJ linewidth when the stand-alone Δf_A linewidth, measured at the −3 dB level, is smaller than the PLL control bandwidth. Figure 12a

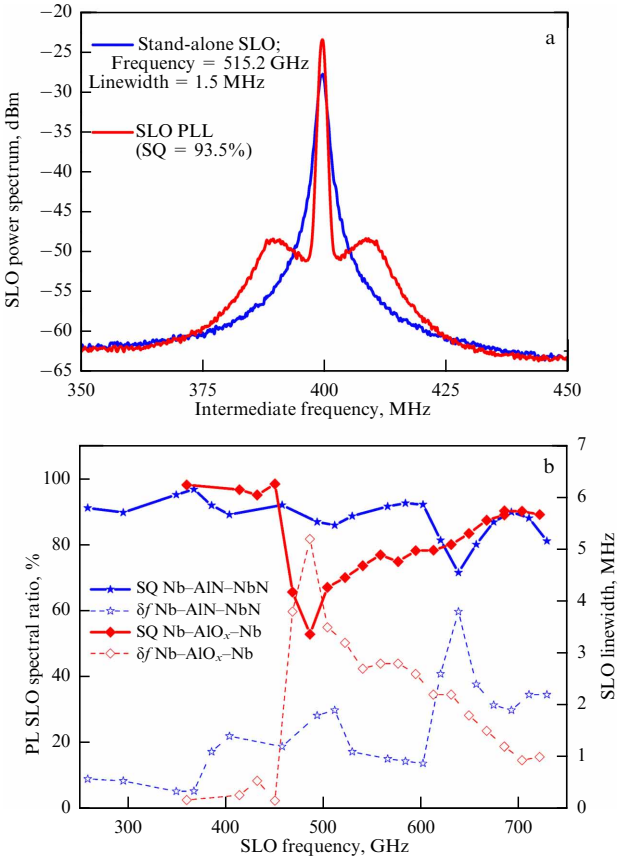

Figure 12. (a) SLO spectra at 515.2 GHz (blue curve — frequency stabilization, red curve — SLO phase stabilization). Linewidth is 1.5 MHz; signal-to-noise ratio SNR = 36 dB; spectral quality SQ = 93.5%. Measurements were performed with a resolution bandwidth of 1 MHz in the range of ±50 MHz from the carrier frequency [72]. (b) Frequency dependence of optimized SLO linewidth and SLO spectral quality in PLL mode. Data are presented for two types of DJJ-based SLO: Nb–AlO_x–Nb (diamonds) and Nb–AlN–NbN (asterisks) [47].

shows the DJJ power spectrum in phase-locked mode with a resolution bandwidth of the spectrum analyzer of 1 MHz. The DJJ linewidth in PLL mode can be reduced significantly below the value determined by shot noise and thermal fluctuations of the tunnel junction in the stand-alone mode and, when measured relative to a reference synthesizer, is only limited by the spectrum analyzer resolution. The phase synchronization results in the appearance of a vertical step ($R_d^B = 0$) on the $I-V$ characteristic of the DJJ at a voltage corresponding to the frequency at which the DJJ is synchronized; the size of this region in current is a few μA; it is determined by the control bandwidth of the PLL system and the differential resistance of the DJJ at the operating point.

To ensure the stability of phase synchronization of the SLO, a sufficiently high value of spectral quality (SQ) is required. This parameter is defined as the ratio of the power at the carrier frequency to the total power radiated by the generator. The values of the autonomous linewidth measured in the range of 250–750 GHz were from 0.5 to 7 MHz, which allows synchronizing from 95% to 35% of the power radiated by the SLO, respectively (Fig. 12b).

To effectively synchronize the superconducting local oscillator operating as part of the integrated spectrometer of the sub-THz range, the concept of a cryogenic phase-locked loop system was proposed and tested, the key element of which is a new element of superconducting electronics — a cryogenic phase detector [75, 76]. The quasiparticle and Josephson modes of operation of the cryogenic harmonic phase detector (CHPD) based on the SIS junction were investigated, and it was found that the Josephson mode is preferable when using the CHPD in a PLL system. Due to the compactness and small delays of the loop, the synchronization bandwidth of the system at about 70 MHz was achieved. The implemented PLL system allows synchronizing more than 90% of the generator radiation power with a linewidth of 12 MHz, which is seven times greater than provides the semiconductor PLL system.

A THz radiation source based on the DJJ, radiating a signal into open space, was developed and investigated. The DJJ was integrated with a transmitting slot antenna on a single microcircuit [97–100]; the microcircuit is placed on the surface of a collecting elliptical silicon lens, so the antenna is located exactly at the focus of the lens. For phase synchronization of the DJJ, a portion of the output power was fed to the HM (based on an SIS mixer with an area of 1.4 μm^2) via an additional microstrip transmission line placed parallel to the line of transmission to the transmitting antenna. The HM output signal at an intermediate frequency of 0–800 MHz, which is a convolution of the DJJ signal and the nth harmonic of the reference synthesizer, is fed into a feedback loop with a PLL system, which phase-synchronizes the signal with a 400-MHz reference oscillator. The power of such a source radiated into open space was measured over the entire operating frequency range for various oscillator designs [101, 102]. For uncalibrated output power measurements, a semiconductor bolometer cooled to 4.2 K, located in a vacuum flooded cryostat, was used. An assessment of the power radiated into open space shows that the characteristic power of DJJ radiation into open space is about 1 μW and significantly depends on the design of the transmitting path; the peak power can reach several μW. Thus, the efficient operation of a DJJ as an external terahertz generator was demonstrated for practical applications where wide frequency tuning and high quality of the spectral line are required with no special requirements regarding the high power of the signal.

4.2 Superconducting integrated receiver

Successful development and practical implementation of individual elements of the THz-range receiver based on the SIS mixer made it possible to start developing a fully superconducting integrated receiver. Scientists from the Kotelnikov Institute of Radio Engineering and Electronics of the Russian Academy of Sciences proposed and tested the concept of a superconducting integrated receiver (SIR) [77, 103, 104]. The device implements a fundamentally new approach: integration of a superconducting heterodyne generator with a quantum mixer based on the quasiparticle nonlinearity of tunnel SIS junctions and a superconducting antenna in a single microcircuit. The SIR chip contains a superconducting planar receiving antenna, a superconducting heterodyne generator, an SIS mixer with two tunnel junctions with an area of 0.8 μm^2 each, and a harmonic SIS mixer used in the phase-locked loop system to stabilize the SLO frequency. When supplied with only constant power from batteries, the microcircuit of such a receiver operates as a superheterodyne receiver in the submillimeter wave range, without requiring any bulky additional microwave equipment. The microcircuit is produced on a 0.5-mm-thick silicon substrate using state-of-the-art microelectronics methods and

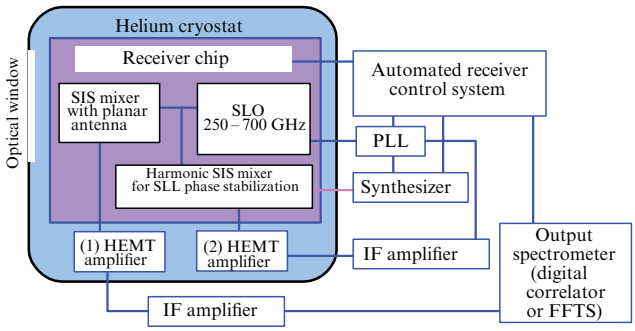

Figure 13. Block diagram of a superconducting integrated receiver [107].

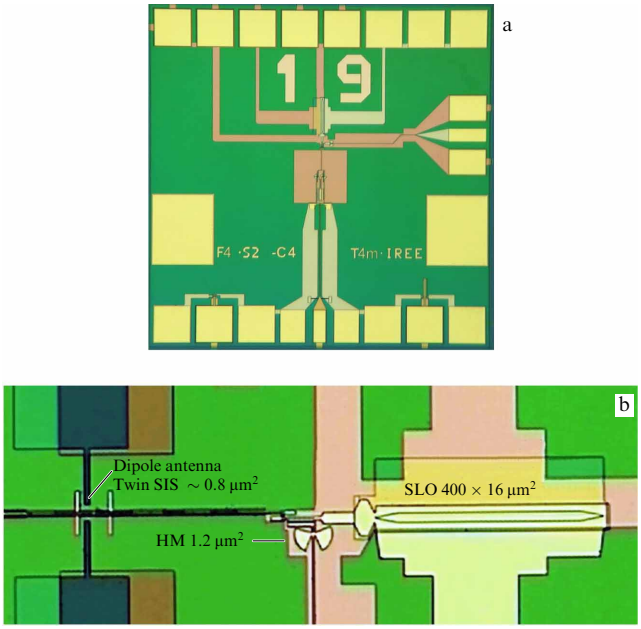

Figure 14. (a) Image of a superconducting integrated receiver microcircuit with a double slot antenna [108]. (b) Photomicrograph of central part of SIR with a double dipole antenna [108].

contains an immersion lens dipole or slot antenna for feeding a signal to a superconducting SIS mixer. The size of the microcircuit with contact pads is 4 × 4 mm. The integration of superconducting elements into a single device made it possible to implement a unique combination of mass, size, and frequency characteristics, which is still unique in the world.

A basic block diagram of a receiver for measuring the spectral distribution of an external electromagnetic signal is presented in Fig. 13 [107], and images of the receiver chip, in Fig. 14 (general view and central part) [108]. The image of the central part (Fig. 14b) displays a DJJ-based SLO measuring 400 × 16 μm^2, a double dipole antenna, an SIS mixer with two submicron junctions, and an HM with an area of approximately 1 μm^2. The radiation of the superconducting local oscillator is transmitted through a matching circuit (impedance transformer) to a microstrip line with an impedance of about 20 Ω, and then, using a power divider (which also separates the mixers and the generator by direct bias current), it is distributed between two SIS mixers.

The integrated receiver microcircuit is mounted on the surface of a silicon lens [108], fixed in a special cryogenic unit, which provides cooling of the microcircuit together with the elements surrounding it and fastening of the board with filters. Radio frequency signals from the microcircuit are transmitted along this board, and the supply currents of the chip are set. Since SLOs are extremely sensitive to magnetic fields, shielding of the SIR microcircuit is necessary. The cryogenic unit consists of two concentric cylinders that provide shielding of the magnetic field. The outer cylinder is made of cryopermalloy, while the inner one is made of copper coated with a 100-μm-thick layer of lead, which passes into a superconducting state. The PCB board is connected to the microcircuit contacts using 25-μm-thick aluminum bonding wires. The cryogenic unit with the board and the receiver microcircuit is placed in a vacuum chamber of a helium cryostat with an optical window; the SIR microcircuit was cooled through aluminum wires 2 mm in diameter, maintaining an operating temperature of about 4.2 K.

The noise temperature of the integrated receiver was determined from the ratio of the signal at the receiver output measured in the hot/cold load switching mode (Y-factor). The best temperature value is less than 120 K at frequencies of around 500 and 610 GHz, and a wide peak is observed in the 570 GHz region, which is partly due to the presence of a water absorption line in the atmosphere and to the properties of the tuning structure integrated with the mixer. For spectral measurements, it is of importance that the noise temperature of the receiver be uniform over the entire intermediate frequency range. To this end, SIR elements were developed and included in the chip design, matching the SIS mixer with the IF path in a wide band (Fig. 14a). Detuning capacitors are located directly on the chip itself, which short-circuit a section of the coplanar line to ground in alternating current, playing the role of a detuning inductor. The latter, along with dividing the coplanar line into two sections, made it possible to increase the IF path bandwidth to 4 GHz and achieve good uniformity of the path amplitude-frequency characteristic in the 4–8-GHz range. The generation frequency is uniquely related to the generator voltage via the Josephson relation. The generation line of the superconducting heterodyne generator has a Lorentz shape with a high degree of accuracy [109, 110] (see the previous section). For an SLO operating as part of an integrated receiver in the frequency range of 500–700 GHz in the frequency stabilization mode, a linewidth of 9 to 2 MHz was achieved, which makes it possible to concentrate 35% to 90% of the power in the central peak using the PLL system in the phase synchronization mode.

For practical studies, it is of importance to know the stability of the integrated receiver, which determines the optimal integration time, the actually achievable measurement time for one integration, and, consequently, the required frequency of the calibration cycle. The stability of the complete SIR system was determined by measuring the receiver output noise fluctuations in the 17-MHz bandwidth [72]. For the two IF channels used to determine the Allan variance, the Allan integration time is about 14 s. If the difference between the two channels is used to determine the Allan variance (the so-called spectroscopic or differential mode), the Allan integration time is 20 s. This is comparable to the stability obtained for the best astronomical receivers. For atmospheric measurements, integration times of about 1 s are usually used, due to the autocorrelator parameters. Thus, SIR stability does not impose any restrictions on the observation strategy.

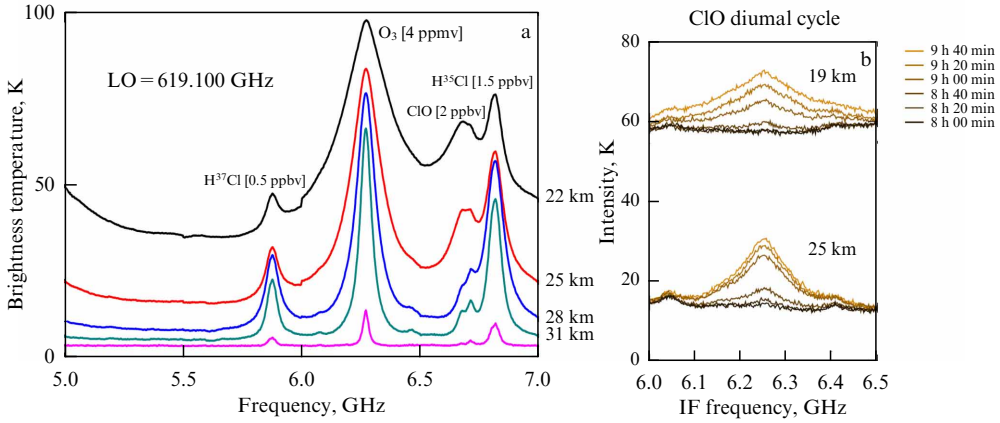

Figure 15. (a) Spectra of two HCl isotopes, ozone, and ClO; local oscillator frequency is 619.1 GHz. Plot shows spectra for a beam touchdown altitude of 22–31 km and a viewing angle of 6°. Corresponding estimated concentrations of observed gases are shown [47]. (b) ClO spectra recorded by SIR (SLO frequency = 507.3 GHz) from an altitude of 34 km. Two sets of spectra correspond to touchdown altitudes of 25 and 19 km, respectively. Increase in ClO with time after sunrise is clearly visible. Received signal intensity is shown on ordinate axis in kelvins [72].

4.3 TELIS project

An SIR-based spectrometer for studying the gaseous components of Earth's atmosphere from a high-altitude balloon was successfully used in the international TErahertz Limb Sounder (TELIS) project [47, 72, 78, 104–108]. The spectrometer was employed to examine the distribution of various compounds in the atmosphere (such as ClO, BrO, O_3, HCl, HOCl, H_2O and its three isotopes, HO_2, NO, N_2O, HNO_3, CH_3Cl, HCN, and many others). The device operates in the limb sounding mode from a high-altitude balloon [47, 72, 78, 107, 108]. Three successful scientific launches of the TELIS spectrometer aboard a high-altitude balloon were carried out together with the MIPAS-B spectrometer. The instrument, which demonstrated its operability under extreme conditions (altitude up to 40 km, temperature minus 90 °C), made it possible to collect a large amount of scientific information confirming the high spectral resolution and sensitivity of the device. Several hundred limb scans were recorded, and spectra of gas components of Earth's atmosphere were registered. Each flight continued for more than 10 hours; measurements were carried out in continuous mode at eight pre-selected frequencies. A wide IF band of 4–8 GHz made it possible to measure the spectra of many dozens of gas components of the atmosphere. In the altitude range of 12–36 km, spectra of isotopes of various substances were also obtained, including isotopes of water and hydrochloric acid (HCl) (Fig. 15a) [47, 111, 112]. The concentrations of the observed gases were estimated; they amounted to 0.5 and 1.5 ppbv for the $H^{37}Cl$ and $H^{35}Cl$ lines, respectively.

During flights of a high-altitude balloon, spectra of chlorine, bromine, and other pollutants responsible for the destruction of the ozone layer in Earth's atmosphere were recorded and daily variations in various atmospheric components were measured. Various chlorine compounds can catalytically destroy the ozone layer. Such destruction of ozone is especially great in the spring in Arctic regions, when the so-called polar vortices cease. As a result, the ClO radical becomes active in significant concentrations. This radical, which has a relatively short lifetime, requires solar radiation for its formation, which leads to daily cyclic changes in its concentration. Figure 15b shows the ClO lines that were measured sunrise [72]. It is evident that the ClO concentration actually increases with time. Bromine is even more active than chlorine in destroying the ozone layer, but its concentration is much lower. For the first time, BrO spectra were detected in the terahertz range; the signal intensity in this case was only 0.3 K [47, 72], which corresponds to an extremely low concentration of several pptv.

A multifunctional automated system, IRTECON (Integrated Receiver TEst and CONtrol), was created to study such complex superconducting structures as the SIR and to control its operation during the flight [113]. The modular design of this system allows its easy adaptation to a wide spectrum of research tasks. The automated system includes advanced libraries for controlling measuring instruments and visualizing experimental data and mathematical algorithms for processing the results. Controlling the SIR in flight consists of constantly monitoring its condition, adjusting the PLL system if necessary, and recovering the system's operating modes after failures. A comprehensive methodology for determining the main characteristics of the SIR, search procedures, and multidimensional optimizations of its operating modes for each selected frequency, and robust algorithms for restoring the SIR operating parameters for both the resonant mode (Fiske steps) and the viscous vortex flow mode, were developed. In total, up to ten SIR control parameters are optimized. All information is recorded in a database and used to set the receiver operating modes in real measurements.

4.4 Laboratory applications of superconducting integrated receiver

A stationary version of the superconducting integrated receiver, developed on the basis of the flight instrument, was successfully used in the laboratory for receiving radiation from new-generation cryogenic generators in the 400–700 GHz range and for spectral analysis of a gas mixture [80, 81, 112, 114]. Using such a spectrometer in the sub-THz range, a series of studies on radiation from superconducting generators based on BSCCO mesa structures was carried out. Oscillators based on superconducting high-temperature structures $Bi_2Sr_2CaCu_2O_{8+\delta}$ (BSCCO) have been actively studied all over the world (both experimentally and theoretically) for the last decade. We were the first to measure the emission spectra of oscillators based on BSCCO mesa structures using a superconducting integrated receiver [80].

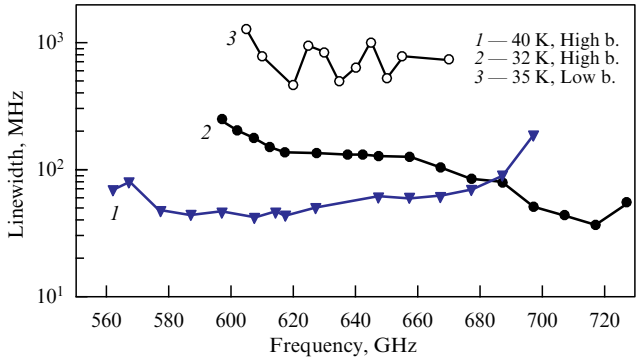

Figure 16. Frequency dependence of generator emission linewidth at various temperatures in low and high bias modes (low and high, respectively) [112].

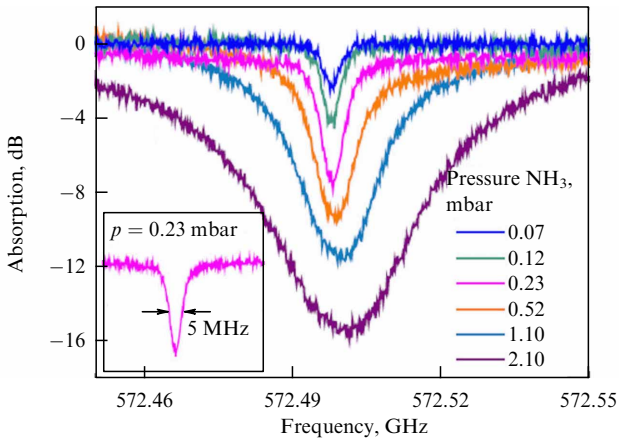

Figure 17. Absorption spectra of ammonia (10% aqueous solution) at various pressures: measurements were carried out using a terahertz radiation generator based on a Josephson transition array (JTA) in BSCCO and a superconducting integrated receiver (absorption in the empty cell is taken into account). Inset shows absorption spectrum of ammonia vapor at $p = 0.23$ mbar with an absorption bandwidth of 5 MHz [80].

Such an oscillator was shown to have the best spectral characteristics in the 'high-bias' mode. Typical values of the BSCCO oscillator linewidth measured in the 'high-current' mode were 10–100 MHz; the shape of the spectral line is Lorentzian with a high degree of accuracy. In the 'low-bias' mode, the structure emits powerful broadband noise with an emission width of about 1 GHz. In the range from 450 to 740 GHz, the spectral characteristics of the emission of high-temperature superconducting (HTSC) mesa structures were measured at temperatures from 4.2 to 55 K (Fig. 16) [112]. In additional experiments, a minimum emission linewidth of 7 MHz and a power of 1–2 μW were obtained [112]. The measurement results showed that the BSCCO oscillator signal can be described by the standard phase-diffusion field model with an exponential correlation function. It should be noted that the emission characteristics of BSCCO oscillators depend on the temperature in the cryostat T_b. The results presented here were obtained for T_b at about 20 K; the temperature was controlled using a special heater installed near the generator. The temperature of the SIR, which was located in another cryostat, was 4.2 K.

For more accurate measurement of the THz absorption spectra of ammonia and water vapor using mesa structures, a superconducting integrated receiver with an effective frequency tuning range from 450 to 700 GHz and a frequency resolution significantly lower than 100 kHz was used. In the experiment, the bias current through the BSCCO generator was kept constant, and it was tuned to generate at the frequency of the corresponding gas line. The intermediate frequency spectra were measured with high accuracy using the SIR. The gas spectra were measured at $T_b = 4.2$ K, where the emitter radiation linewidth is 60 MHz at 572.5 GHz (NH_3) and 57 MHz at 557 GHz (H_2O). Using the SIR [80, 114], the absorption spectra of ammonia (Fig. 17) and water vapor in the THz range were measured with high resolution. The absorption lines of ammonia and water are strongly broadened at high gas pressures; the linewidth decreases with decreasing pressure. For ammonia at $p = 0.23$ mbar, a well-pronounced absorption is observed with an absorption band width of about 5 MHz, as shown in the inset to Fig. 17. At $p = 0.07$ mbar, the measured linewidth was 4 MHz (due to Doppler broadening). The observed frequencies of rotational levels for ammonia (572.498 GHz) and water (556.936 GHz) coincide with the published values.

SIR was used to study human skin radiation at frequencies of 480 and 700 GHz [82]. It was shown that the radiation differs significantly from the expected blackbody signal, the received signal from the skin surface being modulated by the level of mental stress. This observation provide options for remote monitoring of the condition of humans.

5. Conclusions

SIS tunnel junctions are the main elements of most devices and circuits of low-temperature superconducting electronics. The Kotelnikov Institute of Radio Engineering and Electronics of the Russian Academy of Sciences has developed a technology for the production of high-quality $Nb - AlO_x - Nb$ tunnel junctions and multilayer chips containing up to 100 elements. Several new technological processes and methods for the production of superconducting tunnel junctions with record parameters, withstanding more than 10,000 thermal cycles, have been developed. The developed technology for producing high-quality tunnel junctions was used in many fundamental physical studies and experiments. Single-quantum digital devices based on superconducting quantum interferometers were developed and successfully implemented; metamaterials with tunable negative magnetic permeability were created.

Junctions with a high current density J_c allow increasing the operating frequency of SIS receivers and expanding their bandwidth. However, there is a limit to increasing the barrier transparency for SIS junctions based on aluminum oxide, which is about 10–15 kA cm^{-2}. With a further increase in current density, the junction quality sharply degrades. To overcome this limitation, a technology was developed for manufacturing Nb/Al–AlN/Nb tunnel SIS junctions with extremely high transparency of the tunnel barrier with acceptable R_j/R_n values by nitriding the Al surface in a plasma RF discharge. This advancement allowed increasing the operating frequency of SIS receivers, expanding their bandwidth, and creating a number of ultra-sensitive receivers in the 100–1000 GHz range.

A superconducting heterodyne generator based on distributed tunnel Josephson junctions was created and studied, and its design was optimized. The characteristics of the superconducting heterodyne generator were examined for

two types of the studied tunnel structures, $Nb-AlO_x-Nb$ and $Nb-AlN-NbN$; the frequency dependence of the emission linewidth was experimentally measured. Continuous frequency tuning of the superconducting generator in the 250–750 GHz range and phase stabilization of the SLO frequency were implemented for the first time; the spectral quality was more than 70% in the entire frequency range of the SLO tuning. The possibility of obtaining phase noise of the order of −90 dBc with a detuning from the carrier frequency of more than 100 kHz was experimentally demonstrated. For efficient synchronization of a superconducting local oscillator generator incorporated in a sub-THz integrated spectrometer, a concept of a cryogenic phase-locked loop system has been proposed and tested. Due to its compactness and small loop delays, a synchronization bandwidth of about 70 MHz has been achieved. The implemented PLL system allows synchronizing more than 90% of the generator's radiation power with a linewidth of 12 MHz, i.e., seven times more than a semiconductor PLL system.

A concept of a superconducting integrated THz receiver has been developed and tested. The main element of the receiver is an integrated microcircuit that includes an SIS mixer with a planar superconducting receiving antenna, SLO, and a harmonic mixer for phase synchronization of the local oscillator frequency. The onboard integrated receiver features a frequency range of 450–650 GHz, a noise temperature of less than 120 K (DSB), an IF band of 4–8 GHz, and a spectral resolution of better than 1 MHz. Three successful launches of the onboard integrated spectrometer were conducted at the Esrange test site (Sweden). The instrument showed that it can operate under extreme conditions (temperature of −90 °C) and allowed collecting a large amount of scientific information confirming the high spectral resolution and sensitivity of the device at the level of several parts per billion (1 ppb). During flights on a high-altitude balloon, the spectra of various gas components were measured, including ClO and BrO, which are responsible for the destruction of Earth's ozone layer; their distribution was studied in the altitude range of 12–36 km at sunrise; the spectra of isotopes of various substances (H_2O, HCl, etc.) were measured. A laboratory version of an integral spectrometer in the 400–700 GHz range for spectral analysis of a gas mixture has been developed and tested. The high spectral resolution of the device and its extreme sensitivity make it possible to unambiguously measure ultra-low concentrations of a substance by its 'flavor' and create devices for non-invasive medical diagnostics and security systems.

Using the integrated spectrometer created at the Kotelnikov Institute of Radio Engineering and Electronics of the Russian Academy of Sciences, a terahertz generator based on single-crystal HTSC structures $Bi_2Sr_2CaCu_2O_8$ was comprehensively studied. For the first time, spectral characteristics were measured in the range of 450–750 GHz with an accuracy of better than 0.5 MHz; in the 'high bias' mode, the Lorentz shape of the spectral line and high signal stability were demonstrated.

Summarizing, methods for manufacturing superconducting tunnel nanostructures for scientific research and a number of practical applications have been developed. Based on technological research and advancements in creating the elemental base of superconducting electronics, a number of terahertz-range receiving devices with unique parameters were created.

The study was financially supported by the Ministry of Science and Higher Education of the Russian Federation (agreement no. 075-15-2024-538). The development of SIS mixers for the 800–950 GHz range and the technology for their production were supported by a grant from the Russian Science Foundation (RSF) (no. 23-79-00019, https://rscf.ru/project/23-79-00019/). The production and measurement of SIS mixers for the 210–275-GHz range were supported by a grant from the RSF (no. 23-79-00061, https://rscf.ru/project/23-79-00061/).

References

1. Tinkham M *Introduction to Superconductivity* (New York: McGraw-Hill, 1975); Translated into Russian: *Vvedenie v Sverkhprovodimost'* (Translated from English Ed. K K Likharev) (Moscow: Atomizdat, 1980)
2. Barone A, Paternò G (Eds) *Physics and Applications of the Josephson Effect* (New York: Wiley, 1982) https://doi.org/10.1002/352760278X; Translated into Russian: *Effekt Dzhozefsona: Fizika i Primemeniya* (Moscow: Mir, 1984)
3. Likharev K K *Dynamics of Josephson Junctions and Circuits* 3rd ed. (New York: Gordon Breach Sci. Publ., 1996)
4. Clarke J, Braginski A I (Eds) *The SQUID Handbook* Vol. 2 *Applications of SQUIDs and SQUID Systems* (Hoboken: Wiley, 2006) https://doi.org/10.1002/9783527609956
5. Weinstock H (Ed.) *SQUID Sensors: Fundamentals, Fabrication, and Applications* (NATO ASI Series. Ser. E, Vol. 329) (Dordrecht: Kluwer Acad. Publ., 1996)
6. Faley M I et al. *Sensors* **17** 2798 (2017)
7. Huber M et al. *Nucl. Instrum. Meth. Phys. Res. A* **520** 234 (2004)
8. Kozin M G *Izv. Ross. Akad. Nauk Ser. Fiz.* **69** (1) 36 (2005)
9. Semenov A D, Gol'tsman G N, Korneev A A *Physica C* **351** 349 (2001)
10. Gol'tsman G N et al. *Appl. Phys. Lett.* **79** 705 (2001)
11. Pernice W H P et al. *Nat. Commun.* **3** 1325 (2012)
12. Macklin C et al. *Science* **350** 307 (2015)
13. White T C et al. *Appl. Phys. Lett.* **106** 242601 (2015)
14. Aumentado J *IEEE Microw. Mag.* **21** (8) 45 (2020)
15. Likharev K K, Mukhanov O A, Semenov V K "Resistive single flux quantum logic for the Josephson-junction digital technology," in *SQUID'85. Superconducting Quantum Interference Devices and their Applications. Proc. of the Third Intern. Conf. on Superconducting Quantum Devices, Berlin, West, June 25–28, 1985* (Eds D Hahlbohm, H Lübbig) (Berlin: Walter de Gruyter, 1985) p. 1103, https://doi.org/10.1515/9783110862393.1103
16. Likharev K K, Semenov V K *IEEE Trans. Appl. Supercond.* **1** (1) 3 (1991)
17. Koshelets V et al. *IEEE Trans. Magn.* **23** 755 (1987)
18. Filippenko L V et al. *IEEE Trans. Magn.* **27** 2464 (1991)
19. Rey-de-Castro R C et al. *IEEE Trans. Appl. Supercond.* **11** 1014 (2001)
20. Klenov N V et al. *Low Temp. Phys.* **43** 789 (2017); *Fiz. Nizk. Temp.* **43** 991 (2017)
21. Tucker J R, Feldman M J *Rev. Mod. Phys.* **57** 1055 (1985)
22. Zmuidzinas J, Richards P L *Proc. IEEE* **92** 1597 (2004)
23. ALMA Observatory, https://www.almaobservatory.org/en/about-alma/
24. Herschel Space Observatory, https://www.herschel.caltech.edu/
25. Wolf E L et al. (Eds) *Josephson Junctions. History, Devices, and Applications* (New York: Jenny Stanford Publ., 2017) https://doi.org/10.1201/9781315364520
26. Tucker J *IEEE J. Quantum Electron.* **15** 1234 (1979)
27. Richards P L et al. *Appl. Phys. Lett.* **34** 345 (1979)
28. Kerr A R, Feldman M J, Pan S-K "Receive noise temperature, the quantum noise limit, and the role of the zero-point fluctuations," in *Proc. of the Eighth Intern. Symp. on Space Terahertz Technology, Cambridge, MA, USA, 25–27 March 1997* (Eds R Blundell, E Tong) (Cambridge, MA: Harvard Univ., 1997) p. 101
29. De Graauw Th et al. *Astron. Astrophys.* **518** L6 (2010)
30. IRE im. V.A. Kotelnikova RAN. Unikal'naya nauchnaya ustanovka "Kriointegral" — "Tekhnologicheskii i izmeritel'nyi kompleks

dlya sozdaniya sverkhprovodnikovykh nanosistem na osnove novykh materialov" (Kotelnikov IRE RAN. Unique Research Installation "Cryointegral": "Technological and measurement complex for the development of superconducting nanosystems based on mew materials"), https://nanolith.ru/unu.html; http://ckp-rf.ru/usu/352529/
31. Filippenko L V et al. *IEEE Trans. Appl. Supercond.* **11** 816 (2001)
32. Dmitriev P N et al. *IEEE Trans. Appl. Supercond.* **13** 107 (2003)
33. Rudakov K I et al. *Appl. Sci.* **11** 10087 (2021)
34. Monaco R et al. *Phys. Rev. Lett.* **96** 180604 (2006)
35. Kostyurina E A et al. *J. Commun. Technol. Electron.* **62** 1306 (2017); *Radiotekh. Elektron.* **62** 1142 (2017)
36. Butz S et al. *Opt. Express* **21** 22540 (2013)
37. Jung P et al. *Nat. Commun.* **5** 3730 (2014)
38. Rowell J M, Gurvitch M, Geerk J *Phys. Rev. B* **24** 2278 (1981)
39. Gurvitch M, Washington M A, Huggins H A *Appl. Phys. Lett.* **42** 472 (1983)
40. Golubov A A et al. *Phys. Rev. B* **51** 1073 (1995)
41. Dmitriev P N et al. *IEEE Trans. Appl. Supercond.* **9** 3970 (1999)
42. Imamura T, Shiota T, Hasuo S *IEEE Trans. Appl. Supercond.* **2** 1 (1992)
43. Imamura T, Hasuo S *IEEE Trans. Appl. Supercond.* **2** 84 (1992)
44. Kleinsasser A W, Mallison W H, Miller R E *IEEE Trans. Appl. Supercond.* **5** 2318 (1995)
45. Kawamura J et al. *Appl. Phys. Lett.* **76** 2119 (2000)
46. Torgashin M Yu et al. *IEEE Trans. Appl. Supercond.* **17** 379 (2007)
47. Dmitriev P N, Filippenko L V, Koshelets V P "Applications in superconducting SIS mixers and oscillators: Toward integrated receivers," in *Josephson Junctions. History, Devices, and Applications* (Eds E L Wolf et al.) (New York: Jenny Stanford Publ., 2017) pp. 185–244, Ch. 7
48. Rai-Choudhury P (Ed.) *Handbook of Microlithography, Micromachining, and Microfabrication* Vol. 1 *Microlithography* (Bellingham, WA: SPIE, 1997) https://doi.org/10.1117/3.2265070
49. Nanoengineering EBL Tool: eLINE Plus|RAITH Group (2021), https://www.raith.com/product/eline-plus/
50. Greve M M, Holst B *J. Vac. Sci. Technol. B* **31** 043202 (2013)
51. Fominsky M Yu et al. *Electronics* **10** 2944 (2021)
52. Jackson B D et al. *J. Appl. Phys.* **97** 113904 (2005)
53. Karpov A et al. *IEEE Trans. Appl. Supercond.* **17** 343 (2007)
54. Uzawa Y et al. *IEEE Trans. Appl. Supercond.* **25** 2401005 (2015) https://doi.org/10.1109/TASC.2014.2386211
55. Khudchenko A et al. *IEEE Trans. Terahertz Sci. Technol.* **6** 127 (2016)
56. Event Horizon Telescope. Press Release (April 10, 2019): Astronomers Capture First Image of a Black Hole, https://eventhorizontelescope.org/press-release-april-10-2019-astronomers-capture-first-image-black-hole
57. Akiyama K et al. *Astron. Astrophys.* **681** A79 (2024)
58. The Event Horizon Telescope, https://eventhorizontelescope.org/
59. LLAMA — Large Latin American Millimeter/submillimeter Array, https://www.llamaobservatory.org/
60. Radboud University. Africa Millimetre Telescope — AMT, https://www.ru.nl/en/research/research-projects/africa-millimetre-telescope
61. Millimetron. Millimetron Space Observatory. Accessed on March 01, 2024, https://millimetron.ru/index.php/en/
62. Novikov I D et al. *Phys. Usp.* **64** 386 (2021); *Usp. Fiz. Nauk* **191** 404 (2021)
63. Baryshev A M et al. *Astron. Astrophys.* **577** A129 (2015)
64. Rudakov K "Development of advanced superconductor–insulator–superconductor mixers for terahertz radio astronomy," Ph.D. Thesis (Groningen, The Netherlands: Univ. of Groningen, 2021) https://doi.org/10.33612/diss.174103493
65. Zmuidzinas J et al. *IEEE Trans. Microw. Theory Tech.* **42** 698 (1994)
66. Belitsky V Yu, Jacobsson S W, Filippenko L V, Kollberg E L *Microw. Opt. Technol. Lett.* **10** 74 (1995)
67. Rudakov K I et al. *Radiophys. Quantum Electron.* **62** 547 (2019); *Izv. Vyssh. Uchebn. Zaved. Radiofiz.* **62** 613 (2019) https://doi.org/10.1007/s11141-020-10001-7
68. Rudakov K I et al. *Radiophys. Quantum Electron.* **59** 711 (2017); *Izv. Vyssh. Uchebn. Zaved. Radiofiz.* **59** 793 (2017) https://doi.org/10.1007/s11141-017-9739-5
69. Khudchenko A et al., in *Proc. of the 28th Intern. Symp. on Space Terahertz Technology ISSTT-2017, Cologne, Germany, 13–15 March, 2017*, pp. 87–90
70. Otárola A et al. "Atmospheric transparency at Chajnantor: 1973–2003," ALMA Memos, ALMA Memo #512 (2005) accessed on 19 September 2021; https://library.nrao.edu/alma.shtml
71. Koshelets V P et al. *IEEE Trans. Appl. Supercond.* **13** 1035 (2003)
72. Koshelets V P et al. "Integrated submm wave receiver: development and applications," in *Fundamentals of Superconducting Nanoelectronics* (NanoScience and Technology, Ed. A Sidorenko) (Berlin: Springer, 2011) pp. 263–296, https://doi.org/10.1007/978-3-642-20158-5_10
73. Koshelets V P et al. "Flux flow oscillators for sub-mm wave integrated receivers," was presented at *Applied Superconductivity Conf., ASC-98, Palm Desert Springs, CA, USA, 13–18 September 1998*; *IEEE Trans. Appl. Supercond.* **9** 4133 (1999)
74. Koshelets V P et al. *Rev. Sci. Instrum.* **71** 289 (2000)
75. Khudchenko A V et al. *IEEE Trans. Appl. Supercond.* **17** 605 (2007)
76. Kalashnikov K V, Khudchenko A V, Koshelets V P *Appl. Phys. Lett.* **103** 102601 (2013)
77. Koshelets V P, Shitov S V *Supercond. Sci. Technol.* **13** R53 (2000)
78. de Lange G et al. *Supercond. Sci. Technol.* **23** 045016 (2010)
79. Kiselev O et al. *IEEE Trans. Appl. Supercond.* **21** 612 (2011)
80. Li M et al. *Phys. Rev. B* **86** 060505 (2012)
81. Sun H et al. *Phys. Rev. Appl.* **8** 054005 (2017)
82. Baksheeva K A et al. *IEEE Trans. Terahertz Sci. Technol.* **11** 381 (2021)
83. Varmazis C et al. *Appl. Phys. Lett.* **33** 357 (1978)
84. Joergensen E et al. *Phys. Rev. Lett.* **49** 1093 (1982)
85. Cirillo M, Lloyd F L *J. Appl. Phys.* **61** 2581 (1987)
86. Nagatsuma T et al. *J. Appl. Phys.* **54** 3302 (1983)
87. Nagatsuma T et al. *J. Appl. Phys.* **56** 3284 (1984)
88. Nagatsuma T et al. *J. Appl. Phys.* **58** 441 (1985)
89. Qin J, Enpuku K, Yoshida K *J. Appl. Phys.* **63** 1130 (1988)
90. Ustinov A V, Kohlstedt H, Henne P *Phys. Rev. Lett.* **77** 3617 (1996)
91. Werthamer N R *Phys. Rev.* **147** 255 (1966)
92. Hasselberg L-E, Levinsen M T, Samuelsen M R *Phys. Rev. B* **9** 3757 (1974)
93. Koshelets V P et al. *Phys. Rev. B* **56** 5572 (1997)
94. Gulevich D R, Koshelets V P, Kusmartsev F V *Phys. Rev. B* **96** 024515 (2017)
95. Gulevich D R, Filippenko L V, Koshelets V P *J. Low Temp. Phys.* **194** 312 (2019)
96. Gulevich D R, Koshelets V P, Kusmartsev F V *Phys. Rev. B* **99** 060501 (2019)
97. Kinev N V, Rudakov K I, Baryshev A M, Koshelets V P *Phys. Solid State* **60** 2173 (2018); *Fiz. Tverd. Tela* **60** 2132 (2018)
98. Kinev N V et al. *J. Appl. Phys.* **125** 151603 (2019)
99. Kinev N V et al. *J. Commun. Technol. Electron.* **64** 1081 (2019); *Radiotekh. Elektron.* **64** 970 (2019)
100. Kinev N V et al. *Phys. Solid State* **62** 1543 (2020); *Fiz. Tverd. Tela* **62** 1379 (2020)
101. Kinev N V et al. *IEEE Trans. Terahertz Sci. Technol.* **9** 557 (2019)
102. Kinev N V et al. *Sensors* **20** 7276 (2020)
103. Koshelets V P et al. *Appl. Phys. Lett.* **68** 1273 (1996)
104. Koshelets V P et al. *IEEE Trans. Appl. Supercond.* **15** 960 (2005)
105. Koshelets V P et al. *Radiophys. Quantum Electron.* **48** 844 (2005); *Izv. Vyssh. Uchebn. Zaved. Radiofiz.* **48** 947 (2005)
106. Koshelets V P et al. *Radiophys. Quantum Electron.* **50** 847 (2007); *Izv. Vyssh. Uchebn. Zaved. Radiofiz.* **50** 935 (2007)
107. Koshelets V P et al. *Proc. SPIE* **7854** 78540J (2010) https://doi.org/10.1117/12.868916
108. Dmitriev P N et al. *Usp. Sovremen. Radioelektron.* (5) 75 (2010); https://www.elibrary.ru/ltixzt
109. Koshelets V P et al. *Supercond. Sci. Technol.* **14** 1040 (2001)
110. Koshelets V P et al. *IEEE Trans. Appl. Supercond.* **15** 964 (2005)
111. de Lange A et al. *Atmos. Meas. Tech.* **5** 487 (2012)
112. Koshelets V P et al. *IEEE Trans. Terahertz Sci. Technol.* **5** 687 (2015)
113. Ermakov A B et al. *IEEE Trans. Appl. Supercond.* **11** 840 (2001)
114. Kinev N V et al. *Radiophys. Quantum Electron.* **56** 582 (2014); *Izv. Vyssh. Uchebn. Zaved. Radiofiz.* **56** 647 (2013)